Direct observations of shape fluctuation in long-time atomistic simulations of metallic nanoclusters

Rao Huang*
Theoretical Division T-1, Los Alamos National Laboratory, Los Alamos, New Mexico 87545, USA
and Department of Physics, Xiamen University, Xiamen 361005, China

Yuhua Wen
Department of Physics, Xiamen University, Xiamen 361005, China

Arthur F. Voter and Danny Perez†
Theoretical Division T-1, Los Alamos National Laboratory, Los Alamos, New Mexico 87545, USA

(Received 14 June 2017; revised manuscript received 15 November 2018; published 26 December 2018)

Metallic nanoclusters are functional materials whose unique physical and chemical properties are sensitively controlled by their shapes and structures. An in-depth understanding of their morphological stability is therefore of crucial importance. It has been well documented by transmission electron microscopy (TEM) studies that metallic nanoclusters can interconvert between different isomers. However, the relevant mechanisms remain elusive because the timescales of such shape fluctuations are too short to be resolved experimentally and yet too long for conventional atomistic simulations. By employing massively parallel accelerated molecular dynamics (AMD) simulations reaching timescales of milliseconds, we provide a clear description of the dynamical processes leading to shape fluctuation in metallic nanoclusters of platinum, silver, copper, and gold at different sizes and temperatures. In all these materials, direct transformations between face-centered-cubic and fivefold symmetric structures (decahedron or icosahedron) are observed away from the melting point. These transitions occur following either a slip-mediated twinning mechanism or a surface-reconstruction driven process. The identified pathways are shown to be reversible, allowing for genuine shape fluctuation processes that do not involve melting or other external factors.

DOI: 10.1103/PhysRevMaterials.2.126002

I. INTRODUCTION

Owing to the tunability of their properties through the control of their shapes and sizes [1], metallic nanoclusters are increasingly found in a variety of technological applications. When determining the final outcome of the synthesis of these nanoclusters, thermodynamic stability acts as a useful, yet often insufficient, guiding principle. Indeed, because of their complex energy landscapes, kinetic considerations are often critical [2]. Further adding to the complexity is the fact that competing morphologies can be thermally accessible from one another on experimentally relevant timescales, especially in the small-size regime. This gives rise to structural fluctuations going back and forth between different isomers, a phenomenon that has been well documented by numerous transmission electron microscopy (TEM) studies [2–6]. In these experiments, supported metallic nanoclusters periodically transform between face-centered-cubic (fcc) and structures with fivefold symmetry such as icosahedron and decahedron. These fluctuations in turn significantly affect the properties of the system, such as their catalytic activity [7,8], mechanical behavior [9], and optical properties [10]. As the ability to synthesize intricate shapes constantly improves, understanding the factors that affect shape stability is increasingly crucial to ensure that clusters retain their favorable properties in operating conditions.

Despite the ubiquity of shape fluctuations, the underlying mechanisms have remained elusive; indeed, while the waiting times between transitions are typically long, transitions themselves occur too rapidly to be directly imaged [3]. This has led to a number of competing explanations, including melting and recrystallization [11,12], electronic effects due to the TEM beam [13], substrate effect [14], or the so-called quasimelting theory, which involves dislocation-mediated twin nucleation processes [15–17]. In the absence of definitive experimental evidence, computer simulations appear ideally positioned to shed light on the problem. While molecular dynamics (MD) in principle provides fully spatiotemporally resolved transition pathways, it suffers from its own timescale limitations that make simulation times in excess of microseconds (μs) difficult to achieve. Consequently, most MD simulations focus on temperatures close to melting where shape fluctuations can be observed on short timescales. There, transitions to icosahedra have been observed as a precursor to melting [18,19] and simulations suggest that shape changes can occur following partial melting and recrystallization within the solid-liquid coexistence region [17]. In this regime, however, shape fluctuations occur on subnanosecond timescales, indicative of activation barriers of order k_BT or less. This is inconsistent with the observed lifetimes of different isomers in TEM

*huangrao@xmu.edu.cn
†danny_perez@lanl.gov

 ©2018 American Physical Society

experiments (fractions of seconds). Solid-state routes are also known; for example, a direct, highly concerted, transition pathway between cuboctahedron (fcc) and icosahedron has been discovered, but the predicted lifetime of cuboctahedral structures would again be too short to be experimentally captured if that pathway was active [20]. (For completeness, this process is reported in Supplemental Figs. 1 and 2 [21].) A possible explanation is that this process only operates from a relatively narrow range of shapes, and is therefore inhibited in most cases. Therefore, despite sustained interest since the first observation of shape fluctuations over 30 years ago, pathways that are fully consistent with experimental conditions have yet to be conclusively identified. Beyond the fundamental interest of the problem, this uncertainty also makes the rational design of especially shape-stable nanoclusters more difficult.

We reconsider the problem using parallel trajectory splicing (ParSplice) [22], an accelerated MD [23] technique that allows for long, unbiased, atomistic simulations. As detailed in the Methods section, this technique allows for the simulation of the evolution of nanoclusters over timescales of milliseconds (ms). This extension in timescales has enabled the direct observations of pathways between fcc and fivefold-symmetric structures (decahedron or icosahedron) in platinum, silver, copper, and gold, and for a range of different sizes and temperatures; these pathways are in remarkable qualitative agreement with the existing TEM observations. As elaborated below, the results point the role of bulklike partial-dislocation-mediated processes in nucleating multiply twinned structures in fcc. The simulations also identify complex surface reorganizations as a source of the formation and proliferation of fivefold structures. The results demonstrate that both surface and bulklike mechanisms contribute to shape fluctuations away from the melting point.

II. METHODS

Simulations were carried out using ParSplice [22], a recently introduced accelerated MD method [23]. ParSplice parallelizes the generation of trajectories in the time domain, allowing for the use of parallel computers to simulate the evolution of small systems over long timescales, which is not possible with traditional domain decomposition techniques. The key idea in ParSplice is that the trajectory of a system that evolves through sequences of thermally activated transitions can be factorized into a number of "segments" that can be independently generated in parallel and then spliced end-to-end. Each segment is a section of an MD trajectory such that the system remained for at least a time τ_c within the same state before the beginning of the segment and remained for least a time τ_c within the same (but possibly different from the initial) state. Physically, τ_c should be set to the timescale required for trajectories to achieve quasiequilibrium within states, conditional on not escaping [24]; this time is a function of the properties of the state and of the thermostat used (here a stochastic Langevin thermostat). This construction exploits the separation of timescale between local relaxation within a state and escapes from a state to ensure that no information relevant to the statistical prediction of the next escape from a state is lost by stitching independently generated segments solely based only on their end states, even though the location of the segment end points in the full configuration space will not be identical. In particular, this removes the dependence of the statistical properties of the segments on the precise phase-space coordinates used to initialize it. At a conceptual level, ParSplice exploits the same physics that allows transition rates for rare events to be estimated by running large numbers of independent trajectories: when events are sufficiently rare, trajectories quickly lose the memory of their initial conditions and become statistically equivalent with respect to predicting the time and nature of the next transition event. In ParSplice, these statements are made precise through the theory of quasistationary distribution [24]. For additional details, the reader is referred to the original paper [22].

In the following, states are defined as basins of attraction of local minima of the potential energy surface in the full 3N-dimensional configuration space; there is, therefore, no *a priori* assumption on the possible states of the systems and transition mechanisms between these states. For the current state definition, τ_c is controlled by vibrational relaxation [25], and so 1 ps is an appropriate value. ParSplice has previously demonstrated the ability to simulate the evolution of nanoclusters over hundreds of microseconds [26,27]; these timescales are here extended into the milliseconds by deploying the method on tens of thousands of cores on massively parallel computing platforms.

The main strength of ParSplice is that it is extremely accurate and unbiased. It has formally been shown that segments prepared according to the prescription given above can be spliced end-to-end to create a long state-to-state trajectory up to an error that is exponentially small in τ_c [22,24], i.e., ParSplice trajectories are statistically representative of those that would be observed in standard MD, so long as τ_c is properly set. This result holds no matter how states are defined. It is also important to note that the accuracy of the trajectory is independent of the choice of the states in which segments are generated, as (i) a given segment can only be spliced into the trajectory once and (ii) a segment can only be spliced into the trajectory if it starts in the state where the trajectory currently ends. Therefore, a segment generated in dynamically irrelevant states will not be spliced, which minimizes the efficiency of the simulation but does not affect the accuracy of the trajectory. The simplest segment generation strategy would be to dynamically initialize short segments at the current end of the spliced trajectory. In practice, ParSplice tries to predict where the trajectory is likely to spend time in the near-future to avoid generating too many segments at the current end. This prediction is continually reassessed to adjust the distribution of states in which segments are generated. The efficiency of this speculative execution strategy has recently been analyzed for simulations similar to the ones presented here [27].

The main strength of ParSplice is its extremely high dynamical fidelity. This positions the methods favorably compared to other techniques with regards to accuracy. For example, it is possible to enhance sampling or to steer the dynamics by relying on low-dimensional reaction coordinates. These approaches, however, provide no guarantees of dynamical fidelity even if they provide correct thermodynamics, i.e., while the relative probability of the system being found at different values of the reaction coordinate can be recovered, rigorous statements generally cannot be made regarding how

the system evolves between these points. This makes the interpretation of transition pathways observed during such simulations delicate, as biases introduced by the choice of reaction coordinates cannot easily be detected or corrected for. Another strength of ParSplice is that its accuracy does not rely on complete sampling of all possible transition pathways: by splicing segments only once, one can guarantee that the trajectory is statistically correct even if only a small fraction of the state space of the system was explored. Of course, these enviable properties come at a steep computational price as ParSplice only provides a computational speedup in terms of wall-clock time, but not when measured in terms of aggregate CPU time, in contrast to some of the aforementioned methods. This typically constrains the number of trajectories that can be generated in practice, limiting the reach of statistical statements (mean transformation time, large-deviation statistics, etc.) that can be made from simulations. However, the quality of each trajectory makes ParSplice an ideal tool to discuss the nature of the transition pathways, which is the focus of the current paper. Because of the high computational cost of the simulations, we therefore restrict our analysis to the general nature of the pathways, and avoid statistical statements on their relative efficiencies in different conditions.

III. RESULTS

A. Summary of the simulations

Table I summarizes the simulations that were performed. Metallic nanoclusters of Pt, Cu, Au, and Ag, containing either 146, 170, 190, or 231 atoms were considered; 146 and 231 are magic numbers for octahedra; 146 is also one atom short of a perfect Mackay icosahedron, while 170 and 190 are nonmagic numbers. These four elements were chosen to assess whether shape fluctuation mechanisms are robust across a range of different metals and because of the availability of affordable and reasonably accurate embedded atom method (EAM) potentials [28–31]. Calculations were carried out at different temperatures generally not exceeding 75% of the melting temperature of the corresponding nanocluster. We have attempted to lower the temperature as much as possible, while still being able to observe shape fluctuations on ParSplice-accessible timescales (ms). Simulation times range between tens of μs and 4 ms, and between hundreds of thousands and hundreds of millions of transitions were observed in each simulation. These transitions typically connect thousands of topologically unique configurations. By analyzing the structures of the nanoclusters during the relaxation processes, shape fluctuations are identified for all four elements, although not at every size or temperature.

In the following, we focus on the nature of the various pathways linking the fcc and fivefold-symmetric structures. The simulations show that fcc to icosahedron transition can occur directly (through the formation of fivefold surface caps) or through an intermediate decahedral structure, which forms through a slip-mediated twinning mechanism. We also observe a number of cases where fivefold caps appear without inducing transformation of the core of the nanocluster. These two mechanisms are observed to compete even for the same materials and nanocluster sizes, such as in the case of the 170-atom Cu nanocluster (abbreviated as Cu-170 hereafter) at 600 K. These different pathways will be analyzed in detail in the following sections.

B. Thermodynamics

The thermodynamics of small metallic nanoclusters are now well understood: at these sizes, energetics are dominated by surface-energy contributions that stabilize structures rich in {111} facets, at the expense of internal defects or strain. For example, the putative ground state of the Pt nanocluster with 146 atoms is a Marks decahedron; however, considering the role of entropy, the icosahedron will be the free-energy minimum at higher temperatures, owing to softer phonons [32,33]. In comparison, fcc-like configurations are energetically unfavorable, both due to their relatively large surface-energy contributions and stiffer phonons. The calculated free and potential energies of different isomers for the Pt-146 and Pt-147 systems are presented in Supplemental Fig. 3 [21]. As seen from the results, various metastable states of different symmetry are thermally accessible, which opens the door to dynamical shape fluctuation between competing configurations. The other systems examined in this paper are expected to behave essentially in the same way.

C. Dynamics

Of all the simulations performed, the Cu-170 nanocluster at 600 K displays the richest set of shape fluctuations. In the $\sim$22 μs-long trajectory, more than 1 million transitions occurred among 144,713 unique states. The structural evolution of the nanocluster, as characterized by a common neighbor analysis (CNA) [34], is reported in the upper panel of Fig. 1; "421" bonds are representative of fcc-like environments, "422" bonds of local hcp order (stacking faults, twins), and "555" bonds of local icosahedral order. The state-to-state trajectory is also analyzed using the Perron cluster cluster analysis (PCCA) algorithm [35]. PCCA decomposes the visited state-space into clusters that are internally well connected from a kinetic perspective, i.e., PCCA clusters are such that mixing within a cluster is fast compared to escaping from the cluster. This analysis provides a compact and interpretable representation of the dynamics in materials, as it differentiates the kinetically significant transitions by which the structure significantly evolves from repetitive local transitions within a given group of states; cf. Ref. [26] for an example of application to nanoclusters. For this purpose, the visited states are classified into a certain number (N_c) of clusters, which are denoted by different colors. A typical structure of the states in each cluster is illustrated in the lower panel of Fig. 1. Although there is a clear qualitative correlation between PCCA clusters and structural features (i.e., transitions between PCCA clusters are generally accompanied by clear changes in CNA counts), it should be noted that PCCA is based on state-to-state kinetics alone and does not consider structural similarity between states. Therefore, a simple structural interpretation of the clusters is not guaranteed; descriptions of the common features of states within each cluster should therefore be seen as descriptive but not prescriptive of each cluster. Further, note that the

TABLE I. Summary of the simulations.

Element	Number of atoms	T (K)	Trajectory length (ps)	Number of transitions	Number of states	Description
Pt	146	900	70,257,528	162,965	6,246	fcc ⇒ deca ⇒ ico
	170	800	672,396,434	1,937,031	147,377	fcc ⇔ fivefold caps ⇒ ico
		900	20,373,095	240,306	117,680	
	190	800	1,350,168,728	6,630,131	303,572	——
		900	348,662,895	688,027	93,346	fcc ⇒ ico
	231	900	1,986,709,692	4,395,285	252,153	——
		1000	92,171,602	955,401	42,383	
		1100	24,608,419	914,005	110,290	
Cu	146	550	301,832,137	3,942,180	237,293	fcc ⇒ ico
	170	500	4,156,073,707	6,160,286	240,594	——
		550	23,712,165	656,202	241,491	fcc ⇔ fivefold caps ⇒ ico
		600	21,690,608	1,039,065	144,713	fcc ⇒ deca ⇒ ico ⇒ deca ⇒ fcc
	190	500	489,113,720	93,863,998	368,356	——
		600	91,701,072	9,863,950	847,016	
	231	500	438,302,547	49,409	12,817	
		550	66,578,597	4,623,717	262,785	
		600	85,056,822	184,737	169,217	
		700	832,190	237,840	89,356	
Au	146	600	237,233,817	22,910,983	119,489	fcc ⇒ ico
	190	600	521,506,615	10,198,278	85,875	fcc ⇔ fivefold caps
	231	800	774,813,889	795,678	159,743	fcc ⇒ fivefold caps ⇒ helical
Ag	146	500	122,897,307	2,558,937	71,357	——
		550	21,613,546	1,988,646	136,297	fcc ⇔ off-centered fivefold axis
	170	500	841,036,559	1,529,663	258,281	——
		600	128,965,726	3,961,585	616,430	
	190	400	1,651,496,973	2,416,400	60,802	
		500	109,165,848	1,414,790	154,083	
		600	30,620,753	1,091,307	147,863	
	231	500	20,445,451	946,623	92,818	

detailed analysis of the transition pathways presented below is not affected by their assignment to specific PCCA clusters; the clustering analysis is simply used to provide an easily interpretable summary of the evolution of each simulation.

That being said, using $N_c = 9$, most of the PCCA clusters exhibit clear structural signatures. The black cluster corresponds to the neighborhood of the initial fcc structure. It also contains defective fcc configurations, as manifested by the fluctuations in hcp and fcc order. On two occasions, the system enters the red cluster where the system contains multiple stacking faults. After returning to the original group of states, the system acquires a twin boundary that cuts through the center (cf., the blue cluster). This twin quickly transforms into a fivefold axis near the periphery of the nanocluster (cf., the gray cluster); this transition is signaled by an increase in hcp order that corresponds to the formation of the additional twin faults. The fivefold axis then migrates toward the center of the nanocluster, leading to a conventional decahedral shape (in yellow). The system remains in this cluster for $\sim$10 μs before transitioning to defective icosahedral states assigned to the orange cluster; this transition is accompanied by a further increase in local hcp and icosahedral local environments. The system then proceeds to different variants of defective icosahedral states (in cyan). This is an example of an intercluster transition with a weak structural signature. The system finally makes its way back to fcc configurations (in green) through an intermediate cluster (in beige).

This single simulation captures the main shape fluctuation mechanisms observed in all the other simulations reported in Table I. To illustrate the generality of the observed mechanisms, they will now be analyzed in detail based on simulations carried out in various materials, sizes, and temperatures.

1. Twin-mediated formation of fivefold symmetry from fcc

The first major shape fluctuation event in the Cu-170 simulation corresponds to a slip-mediated twinning mechanism that leads to the formation of a fivefold symmetry axis. This mechanism is observed in many systems, including Pt-146, Cu-170, and Ag-146. Figure 2 characterizes the structural evolution of the Pt-146 nanocluster at 900 K. This simulation was initialized from an octahedron and continued

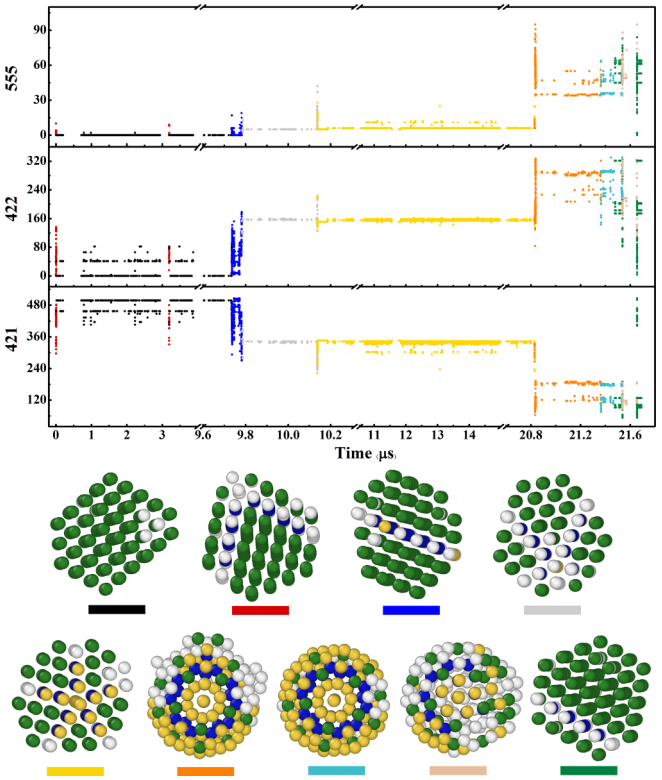

FIG. 1. Structural characterization of the Cu-170 nanocluster during the simulation at $T = 600$ K. Upper panel: Time evolution of the number of various types of bond, as identified by CNA. The data points are colored by their PCCA cluster assignment ($N_c = 9$). Lower panel: Typical structure of states in each PCCA cluster. Colors denote atomic types determined by the CNA signatures as in Ref. [19]: green, fcc atoms; blue, hexagonal close-packed (hcp) atoms; yellow, icosahedral atoms; white, others. This color convention is adopted throughout the paper.

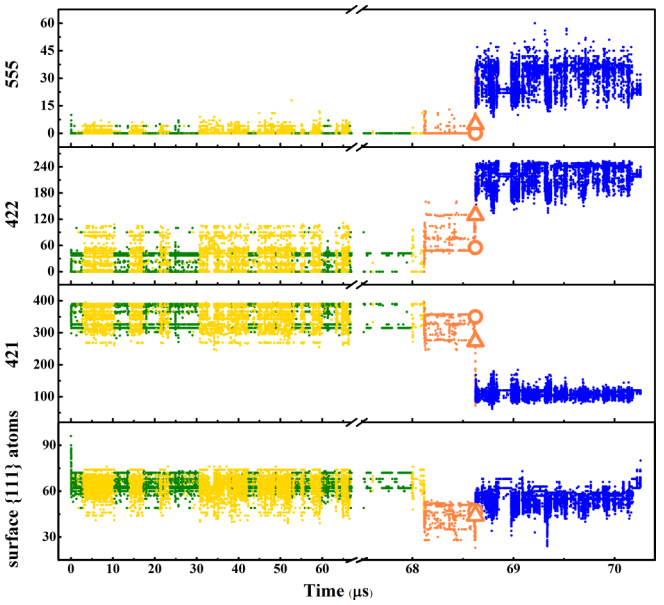

FIG. 2. Time evolution of the CNA counts and of the number of the surface {111} atoms. Colors denote the PCCA cluster assignment of each state ($N_c = 4$). The simulation was performed at $T = 900$ K, began from a perfect Pt octahedron with 146 atoms, and ended in an icosahedral configuration with the central atom missing. Circles and triangles indicate the onset and termination of the process leading to the formation of the first fivefold twin structure, respectively.

up to the formation of an icosahedral nanocluster with the central atom missing (the putative free-energy minimum). In the ∼70 μs-long trajectory, the nanocluster experienced more than 162 000 transitions among 6246 unique states. Structurally, the simulation can be separated into three main phases: exploration of fcc states (corresponding to the green and yellow regions in Fig. 2), formation of a first fivefold twinned structure (the orange region), and, finally, formation of additional fivefold symmetry axes that quickly lead to icosahedral states (the blue region). This last phase follows from complex surface-driven reconstructions, which will be discussed later.

During the first phase, lasting around 68 μs, the system explores different fcc configurations (cf. the fcc band in Supplemental Fig. 3 [21]). This phase is characterized by the near absence of local icosahedral order but by strong fluctuations in the relative amount of fcc and hcp local order. Regions of relatively constant CNA counts correspond to surface reorganization, while large variations in fcc and hcp order signal the nucleation and annihilation of stacking faults and twin planes. As shown in Fig. 2, these plastic deformation modes are extremely active, occurring on a sub-μs timescale.

The initial formation of a stacking fault from a pristine fcc nanocluster occurs following the emission of a $1/6\langle 211\rangle$ partial dislocation that nucleates at a corner and propagates throughout. (The minimum energy pathway and snapshots are reported in Supplemental Fig. 4 [21].) Twinning occurs following a sequence of such events, as shown in Fig. 3. In this case, a stacking fault is initially present close to one of the surfaces of the nanocluster. A second fault then forms on a neighboring {111} plane, through the nucleation and propagation of a $1/6\langle 211\rangle$ partial dislocation (shown in red in the figure), creating an extended {111} faulted region (as seen from snapshots 1 to 5 in Fig. 3). This dislocation-mediated slip process then repeats along the originally faulted plane, leaving a centered twin boundary behind (as seen from snapshots 5 to 8 in Fig. 3). The configurations containing a centered twin boundary are grouped in the orange states in Fig. 2. Their emergence also brings about a significant reduction of the surface {111} atoms, which results from the surface reorganization accompanying the slip. The movement of the surface atoms generates some {100} and {110} facets, replacing the original {111} ones of the initial octahedron.

The appearance of the twin boundary shown in Fig. 4(a) marks the beginning of a second, much shorter phase that leads to the formation of a fivefold twinned structure (a movie showing the evolution along with the corresponding minimum energy pathway is provided in Supplemental Figs. 5 and 6 [21]). This twinned structure [cf. circle markers in Fig. 2(a)] enables a concerted slip process [red arrows in Fig. 4(a)] that leads to the formation of a second twin at the bottom of the nanocluster [cf. Fig. 4(b)]. Another concerted slip of the leftmost layer of the nanocluster [red arrows in Fig. 4(b)] then

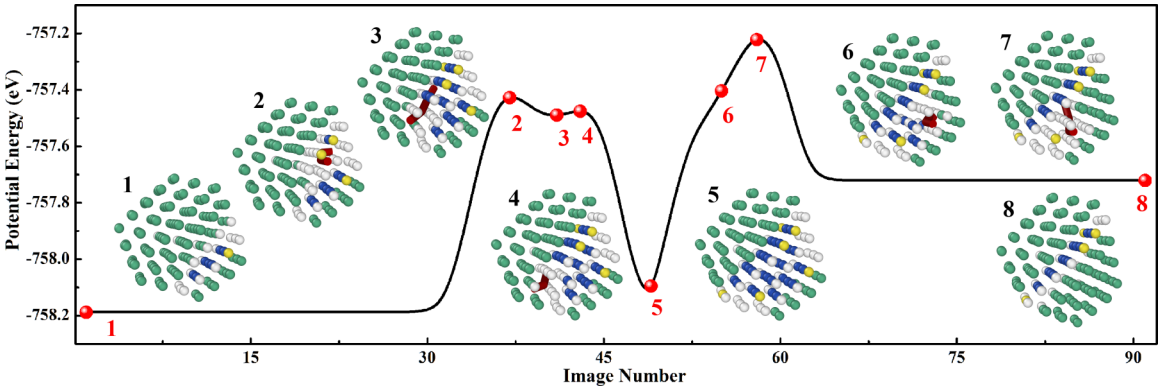

FIG. 3. Minimum energy pathway leading to the creation of a twin boundary through nucleation and propagation of two $1/6\langle 211\rangle$ partial dislocations. A first slip occurs on a plane next to an existing stacking fault, while a second slip anneals the original fault, leading to the formation of a twin plane. The dislocation line, as identified by the DXA algorithm [36], is shown in red.

follows, leading up to the configuration shown in Fig. 4(c). The last step is the expulsion of an atomic column from the intersection of the two twins (left pointing arrow in Fig. 4(c)] by two other columns coming together (up/down arrows). This pinching motion initiates at the front surface and propagates toward the back. This sequence leads to the formation of an off-center fivefold twinned structure [cf. Fig. 4(d) and triangles in Fig. 2(a)]. The activation barriers corresponding to these transitions are relatively high, namely 1.08, 0.854, and 0.709 eV, respectively (cf. Supplemental Fig. 5 [21]). These are, however, accompanied by above-normal harmonic transition state theory prefactors, 4.65×10^{15}, 5.54×10^{14}, 5.90×10^{15} s^{-1}, respectively; these high prefactors entail sub-ns transition times at 900 K. This indicates that the rate-limiting step for the creation of the fivefold structure is the formation of the initial singly twinned state, which required about 68 μs, and not the waiting time to generate the additional twins. This mismatch is a reminder that the overall transition rate from fcc-like states to decahedral-like states cannot be easily inferred from the transition state theory parameters of the last steps alone, as the time needed for the system to reach a state where the pathway is activated can dominate, as it does here. Making accurate predictions of the overall rate would require an exhaustive exploration of the whole state space, which is not guaranteed (nor required by) ParSplice.

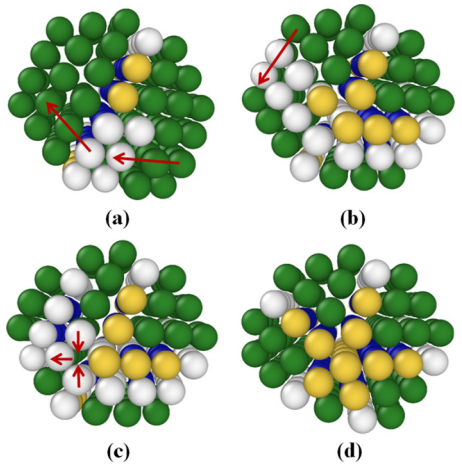

FIG. 4. Process leading to the formation of the first fivefold twinned structure. Panels (a) [corresponding to the circle markers in Fig. 2] through (d) [corresponding to the triangle markers in Fig. 2] show the different energy minima visited along the minimum energy pathway corresponding to this transition.

The transformation pathway for this second phase is quite robust: when starting from the configuration shown in Fig. 4(a), additional ParSplice and MD simulations at different temperatures reliably lead to the formation of a fivefold axis. The simulations on the Cu-170 and Ag-146 also exhibited similar behavior: the trajectory remained trapped in fcc states for quite a long time, until the nucleation of a single twin at the center of the nanocluster led to the formation of a fivefold axis. This is consistent with the fact that multiple stacking faults nucleated and annihilated without leading to the formation of a fivefold axis; only when a twin plane formed in the center of the nanocluster did that transformation follow. This demonstrates how successive bulklike (i.e., dislocation-mediated) slip processes lead to the formation of multiply twinned fivefold structures. Further, barriers of about 1 eV coupled with slightly elevated prefactors correspond to transition times on the order of seconds around room temperature, in agreement with experimental observations.

The reverse of this transformation, leading back to fcc isomers, was also observed in Cu-170 and in Ag-146. As shown in the movie in Supplemental Fig. 7 [21], the reverse process annihilates a fivefold axis and leaves a twin boundary behind. In additional simulations performed in Cu-170 at 600 K, this reverse process was observed frequently, indicating that this twin-mediated route can reliably lead to shape fluctuations between fcc and decahedral structures.

This mechanism differs from that discussed in the context of the quasimelting theory by Marks *et al.* (cf. Fig. 1 of Ref. [15]). To bound the true barrier for transformation, these authors considered a continuous pathway where a fivefold twin structure directly nucleates close to an interface and subsequently translates to the center of the nanocluster; continued propagation of such a fivefold twin to the opposite side of the nanocluster would then leave a twin behind. In contrast, the current simulations indicate that a twin first forms through a

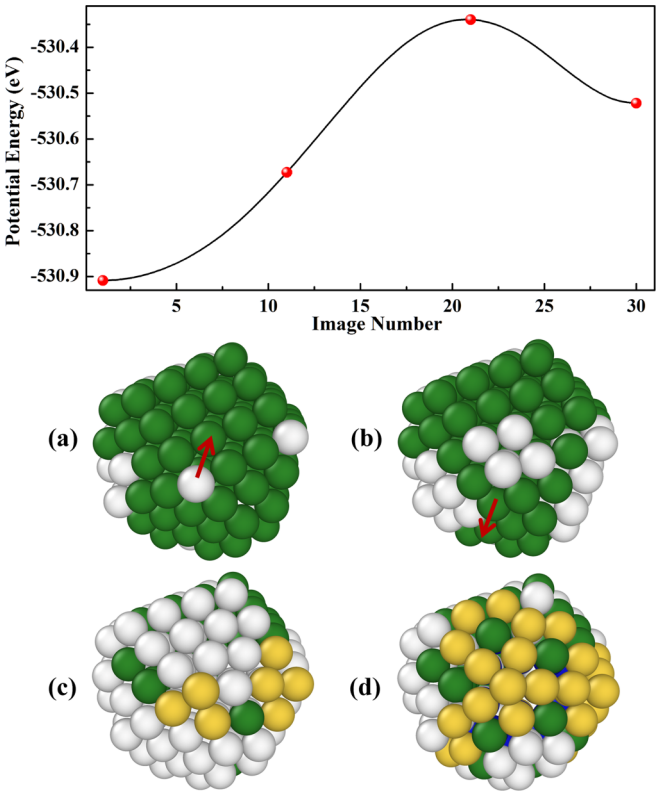

FIG. 5. Upper panel: Minimum energy pathway leading to the creation of fivefold caps through surface reconstruction, taken from the simulation of the Cu-170 nanocluster at 600 K. Lower panel: The snapshots from (a) to (d) respectively correspond to the initial, intermediate, saddle, and final configurations. The directions of atomic movements are indicated by red arrows.

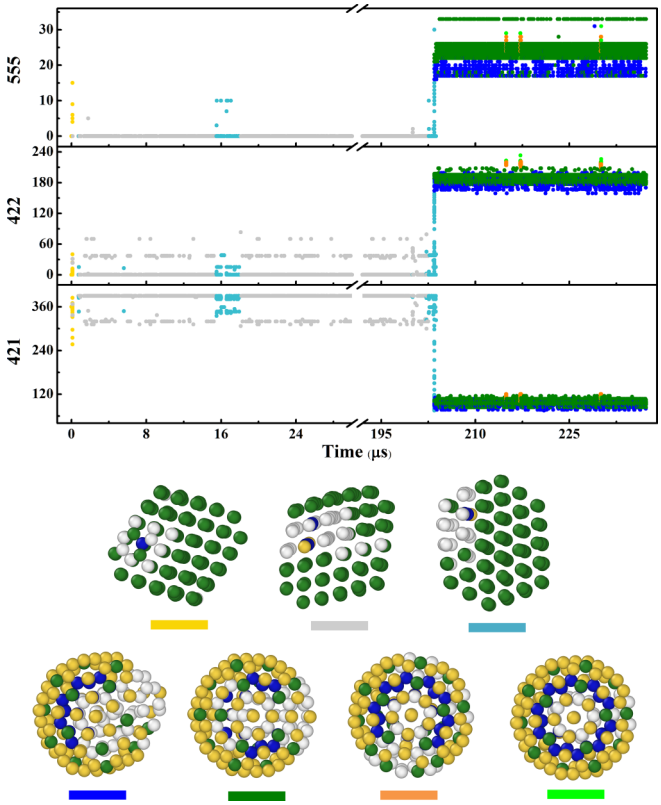

FIG. 6. Structural characterization of the Au-146 nanocluster simulated at $T = 600$ K. Upper panel: Time evolution of the CNA counts. The data points are colored by their PCCA cluster assignment ($N_c = 7$). Lower panel: Typical structure of the states in each PCCA cluster.

slip-mediated mechanism, creating a configuration that allows for additional twins to form, again through slips. The results also differ from recent simulations based on potential energy landscape exploration techniques for small Au clusters that suggested that the transformation pathway from a twinned structure to a decahedral structure involved intermediate disordered states [37]. However, differences could be attributable to the smaller sizes of particles that were the primary focus of that study, or to a contribution from surface-driven pathways which we discuss next.

2. *Surface-reconstruction driven formation of fivefold caps*

The simulations indicate that surface reconstruction provides another pathway to the nucleation of fivefold symmetric structures. While previous simulations have shown that this process operates from decahedral structures [26], Fig. 5 reports the generation of several fivefold caps directly from fcc. This pathway is a section from the end (around 21.66 μs, cf. Fig. 1) of the Cu-170 simulation at $T = 600$ K (the corresponding movie is presented in Supplemental Fig. 8 [21]). New fivefold-symmetric surface caps are formed through the local shearing of {100} facets into compact {111} facets. As shown in Fig. 5, the atom located at the very center of the cap initiates this concerted movement. Further, the nanocluster can be seen to still be mostly made of fcc atoms, as shown in green in the figure. This process shares strong similarities with the first stage of the direct cuboctahedron → icosahedron transition shown in Supplemental Figs. 1 and 2 [21]; the changes are here, however, localized instead of simultaneously occurring over the whole surface. Such so-called diamond-square-diamond transition pathways have often been reported in nanoclusters [20,38]. The barrier for this transition is 0.57 eV, and the corresponding prefactor is very high, at about 3.3×10^{17} s^{-1}. This high prefactor is presumably linked to the softer phonons that thermally stabilize icosahedral configurations (cf. Supplemental Fig. 3 [21]): transitions that increase icosahedral order would therefore tend to show high prefactors. This is clearly illustrated in the case of the direct cuboctahedral to icosahedral transition where the prefactor reaches 10^{21} s^{-1} (cf. Supplemental Material [21]). Again, please note that these barriers and prefactors correspond to the final transformation step, not to the overall pathway.

In some cases (Pt-190, Cu-146, Au-146), the appearance of surface mechanism leads to a very fast transition toward icosahedral states. Triggered by the initial surface reconstruction, the nanoclusters there experience a rapid sequence of highly concerted transitions that further increase the number of fivefold surface caps and eventually lead to the transition of the core. Taking the Au-146 case as representative, the transformation is signaled by the abrupt jump of all the three CNA bond counts around 203 μs (cf. Fig. 6). However,

even the quasicomplete reconstruction of the surface does not imply that the core has fully reconstructed. Often, multiple caps need to properly align before the core changes symmetry. For example, the blue cluster contains states where the surface is mostly composed of {111} facets, but where the core has yet to reconstruct into a perfect icosahedral configuration. This reconstruction gradually proceeds through the green cluster, culminating in the bright green cluster, which contains the perfect icosahedron with the central atom missing (the putative minimum free energy state for this system). In other cases (Pt-170, Cu-170), the complete transition to icosahedra requires multiple attempts where caps nucleate but eventually annihilate before the core reconstructs. In one case (Au-190), core reconstruction was never observed in spite of the repeated formation of fivefold surface caps.

In this case also, the mechanism leading to the formation of icosahedral structures is reversible, allowing for reversible shape fluctuations. As shown in Fig. 1, the surface can spontaneously lose {111} facets and surface caps, leading to the gradual loss of fivefold symmetry in the core (beige cluster). This leads to a decahedral configuration, which then decays back to fcc through the inverse of the twinning mechanism discussed above.

IV. DISCUSSION

Existing experiments have provided qualitative evidence to support the observed slip-mediated mechanism. First, the occurrence of thermally activated nucleation and annihilation of stacking faults and twins is well established experimentally [3,39]. Such events were even shown to dominate the evolution of fcc Au nanoclusters [3], as observed here. That same study captured a sequence of transitions leading to the rapid formation of an off-center fivefold twin from a configuration where the nanocluster is bisected by a single twin through its center (cf. Fig. 4 of Ref. [3]), in almost direct correspondence with the process shown in Fig. 4. The formation of a fivefold axis following the intersection of twins that formed a few layers from free surfaces has also been reported (cf. Fig. 4 of Ref. [39]). These experimental observations suggest that the slip-mediated mechanism can potentially operate for nanoclusters that are significantly larger than those considered here (up to radii of at least 10 nm), and at lower temperatures (e.g., down to 200 °C in Ref. [3]), potentially making this pathway extremely general.

Meanwhile, the surface-reconstruction driven mechanism, which proceeds through the formation of fivefold symmetric caps on the surface, is also supported by both experimental [40] and theoretical [16,41] results showing that growing decahedra can transform into icosahedra through the formation of incomplete external icosahedral shells. The key role of the surface in this reorganization appears natural given that the minimization of the surface energy is the reason why icosahedral nanoclusters are favored in the first place. It is also consistent with previous computational observations that the formation of icosahedral structures upon freezing also begins at the surface and propagates toward the core [42], suggesting that this mechanism could potentially also operate at temperatures closer to melting. However, as the system enters the solid-liquid coexistence region, different mechanisms are likely to start dominating [17,43]. As for the reverse transitions from fivefold symmetric states back to fcc, they are generally observed at larger sizes where the thermodynamic driving force is larger [32]. However, it should be noted that these insights were mostly obtained by simulating the growth process of nanoclusters, in which case the systematic energetic trend leads to short transition times [44,45] as compared to experimental observations.

Our results provide a direct demonstration that shape fluctuations can occur through a sequence of thermally activated processes either mediated by partial dislocations (as hypothesized in Ref. [3]) or triggered by surface reconstruction, without the need for melting [15–17], beam-induced electronic effects [13,46], or interactions with substrates [14]. This, of course, does not rule out the possibility that such factors affect shape fluctuations, which is well established. For example, it has been reported that increasing beam intensity does lead to measurable changes in the shape fluctuation character and dynamics [4,6,46]. The responsible physical mechanisms (e.g., heating vs more complex electronic effects) are, however, not currently fully understood [47].

V. CONCLUSION

Accelerated MD was used to uncover the origin of shape fluctuations in metallic nanoclusters. The simulations, performed for different metals over timescale of up to ms, provide a fully resolved and unbiased description of the transitions between the fcc and icosahedral isomers. We observe two main classes of pathways: a slip-mediated twinning route from fcc to decahedral states, and a surface-mediated creation of fivefold caps that can either operate directly from fcc, or from the decahedral state, and lead to the formation of icosahedral structures. In both cases, these mechanisms were observed to be reversible, allowing for reversible shape fluctuation between the different structures. The identified mechanisms, relying only on thermal activation, are in qualitative agreement with the existing TEM observations.

ACKNOWLEDGMENTS

This work was supported by the United States Department of Energy (DOE) Office of Basic Energy Sciences, Materials Sciences and Engineering Division (D.P., A.F.V.), the China Scholarship Council (R.H.), and the National Natural Science Foundation of China (R.H., Y.W., Grants No. 51871189 and No. 11474234). The development and implementation of the ParSplice code was initially supported by LANL/LDRD Project No. 20150557ER, and currently by DOE/ECP. This research used resources provided by the Los Alamos National Laboratory Institutional Computing Program and by the Tianhe-2 supercomputer in China. Los Alamos National Laboratory (LANL) is operated by Los Alamos National Security, LLC, for the National Nuclear Security administration of the US DOE under Contract No. DE-AC52-06NA25396.

[1] M. M. Mariscal, O. A. Oviedo, and E. P. M. Leiva, *Metal Clusters and Nanoalloys Nanostructure Science and Technology* (Springer, New York, 2013).

[2] L. D. Marks, Rep. Prog. Phys. **57**, 603 (1994).

[3] T. Ben-David, Y. Lereah, G. Deutscher, J. M. Penisson, A. Bourret, R. Kofman, and P. Cheyssac, Phys. Rev. Lett. **78**, 2585 (1997).

[4] R. Wang, H. Zhang, M. Farle, and C. Kisielowski, Nanoscale **1**, 276 (2009).

[5] B. Zhang, D. Wang, W. Zhang, D. S. Su, and R. Schlögl, Chem. Eur. J. **17**, 12877 (2011).

[6] S. Wu, Y. Jiang, L. Hu, J. Sun, P. Wan, and L. Sun, Nanoscale **8**, 12282 (2016).

[7] W. Xu, J. S. Kong, Y.-T. E. Yeh, and P. Chen, Nat. Mater. **7**, 992 (2008).

[8] X. Zhou, W. Xu, G. Liu, D. Panda, and P. Chen, J. Am. Chem. Soc. **132**, 138 (2010).

[9] M. A. Mahmoud, D. O'Neil, and M. A. El-Sayed, Nano Lett. **14**, 743 (2014).

[10] G. T. Bae and C. M. Aikens, J. Phys. Chem. C **119**, 23127 (2015).

[11] P. Williams, Appl. Phys. Lett. **50**, 1760 (1987).

[12] D. Ugarte, Z. Phys. D: At., Mol. Clusters **28**, 177 (1993).

[13] A. Howie, Nature **320**, 684 (1986).

[14] S. Sawada and S. Sugano, Z. Phys. D: At., Mol. Clusters **24**, 377 (1992).

[15] J. Dundurs, L. D. Marks, and P. M. Ajayan, Philos. Mag. A **57**, 605 (1988).

[16] C. L. Kuo and P. Clancy, J. Phys. Chem. B **109**, 13743 (2005).

[17] D. Schebarchov and S. C. Hendy, Phys. Rev. B **73**, 121402 (2006).

[18] C. L. Cleveland, W. D. Luedtke, and U. Landman, Phys. Rev. Lett. **81**, 2036 (1998).

[19] C. L. Cleveland, W. D. Luedtke, and U. Landman, Phys. Rev. B **60**, 5065 (1999).

[20] D. J. Wales and L. J. Munro, J. Phys. Chem. **100**, 2053 (1996).

[21] See Supplemental Material at http://link.aps.org/supplemental/10.1103/PhysRevMaterials.2.126002 for Figs. 1–8.

[22] D. Perez, E. D. Cubuk, A. Waterland, E. Kaxiras, and A. F. Voter, J. Chem. Theory Comput. **12**, 18 (2015).

[23] D. Perez, B. P. Uberuaga, Y. Shim, J. G. Amar, and A. F. Voter, Annu. Rep. Comput. Chem. **5**, 79 (2009).

[24] C. Le Bris, T. Lelievre, M. Luskin, and D. Perez, Monte Carlo Meth. Appl. **18**, 119 (2012).

[25] D. Perez, B. P. Uberuaga, and A. F. Voter, Comput. Mater. Sci. **100**, 90 (2015).

[26] R. Huang, L.-T. Lo, Y. Wen, A. F. Voter, and D. Perez, J. Chem. Phys. **147**, 152717 (2017).

[27] D. Perez, R. Huang, and A. F. Voter, J. Mater. Res. **33**, 813 (2018).

[28] A. F. Voter and S. P. Chen, MRS Online Proc. Library Arch. **82**, 175 (1986).

[29] Y. Mishin, M. J. Mehl, D. A. Papaconstantopoulos, A. F. Voter, and J. D. Kress, Phys. Rev. B **63**, 224106 (2001).

[30] G. Grochola, S. P. Russo, and I. K. Snook, J. Chem. Phys. **123**, 204719 (2005).

[31] P. L. Williams, Y. Mishin, and J. C. Hamilton, Modell. Simul. Mater. Sci. Eng. **14**, 817 (2006).

[32] J. P. K. Doye and F. Calvo, Phys. Rev. Lett. **86**, 3570 (2001).

[33] D. J. Wales and P. Salamon, Proc. Natl. Acad. Sci. USA **111**, 617 (2014).

[34] A. S. Clarke and H. Jónsson, Phys. Rev. E **47**, 3975 (1993).

[35] P. Deuflhard and M. Weber, Linear Algebra Appl. **398**, 161 (2005).

[36] A. Stukowski, V. V. Bulatov, and A. Arsenlis, Modell. Simul. Mater. Sci. Eng. **20**, 085007 (2012).

[37] D. Schebarchov, F. Baletto, and D. J. Wales, Nanoscale **10**, 2004 (2018).

[38] L. Pavan, K. Rossi, and F. Baletto, J. Chem. Phys. **143**, 184304 (2015).

[39] D. J. Smith, A. K. Petford-Long, L. R. Wallenberg, and J. O. Bovin, Science **233**, 872 (1986).

[40] M. R. Langille, J. Zhang, M. L. Personick, S. Li, and C. A. Mirkin, Science **337**, 954 (2012).

[41] F. Baletto, C. Mottet, and R. Ferrando, Phys. Rev. B **63**, 155408 (2001).

[42] H. S. Nam, N. M. Hwang, B. D. Yu, and J. K. Yoon, Phys. Rev. Lett. **89**, 275502 (2002).

[43] D. Schebarchov and S. C. Hendy, Phys. Rev. Lett. **95**, 116101 (2005).

[44] A. A. Tal, E. P. Münger, and I. A. Abrikosov, Phys. Rev. B **92**, 020102 (2015).

[45] D. M. Wells, G. Rossi, R. Ferrando, and R. E. Palmer, Nanoscale **7**, 6498 (2015).

[46] Z. W. Wang and R. E. Palmer, Phys. Rev. Lett. **108**, 245502 (2012).

[47] Y. Lereah, R. Kofman, J. M. Penisson, G. Deutscher, P. Cheyssac, T. B. David, and A. Bourret, Philos. Mag. B **81**, 1801 (2001).